Ultrasonics 125 (2022) 106781

Contents lists available at ScienceDirect

Ultrasonics

journal homepage: www.elsevier.com/locate/ultras

Optimised polymer trapped-air lenses for ultrasound focusing in water exploiting Fabry-Pérot resonance

Lorenzo Astolfi [a], David A. Hutchins [a], Richard L. Watson [b], Peter J. Thomas [a], Marco Ricci [c], Luzhen Nie [d], Steven Freear [d], Timothy P. Cooper [e], Adam T. Clare [e], Stefano Laureti [c,*]

[a] School of Engineering, University of Warwick, Coventry CV4 7AL, UK
[b] Department of Mechanical Engineering Sciences, University of Surrey, Guildford, Surrey GU2 7XH, UK
[c] Department of Informatics, Modelling, Electronics and System Engineering, University of Calabria, 87036 Rende, Italy
[d] School of Electronic and Electrical Engineering, University of Leeds, Leeds LS2 9JT, UK
[e] Department of Mechanical, Material and Manufacturing Engineering, University of Nottingham, University Park, Nottingham NG7 2RD, UK

ARTICLE INFO

Keywords:
Ultrasonics
Trapped-air lens
Fabry-Pérot resonance
Ultrasound focusing
Additive-manufacturing
Polymer
MRI

ABSTRACT

The concept of employing air volumes trapped inside polymer shells to make a lens for ultrasound focusing in water is investigated. The proposed lenses use evenly-spaced concentric rings, each having an air-filled polymer shell construction, defining concentric water-filled channels. Numerical simulations and experiments have shown that a plane wave can be focused, and that the amplification can be boosted by Fabry-Pérot resonances within the water channels with an appropriate choice of the lens thickness. The effect of the polymer shell thickness and the depth of the channels is discussed, as these factors can affect the geometry and hence the frequency of operation. The result was a lens with a Full Width at Half Maximum value of 0.65 of a wavelength at the focus. Results obtained on a metal-based counterpart are also shown for comparison. An advantage of this polymeric design is that it is easily constructed via additive manufacturing. This study shows that trapped-air lenses made of polymer are suitable for ultrasound focusing in water near 500 kHz.

1. Introduction

Ultrasound focusing has been widely studied for biomedical imaging [1,2,3], Nondestructive Testing (NDT) [4,5] and sound regulation applications [6]. Conventional methods for focussing the acoustic field include acoustic mirrors [7] or, more commonly, phased-array transducers [8] or focused transducers [9].

In the last decade, efforts have been made to fabricate artificial structures such as Phononic Crystals (PCs) or Acoustic Metamaterials (AMMs) to manipulate sound in extraordinary ways. These structures are usually made of periodically-arranged scatterers or resonators, engineered to change dispersion-related phenomena through scattering or local resonances [10,11]. It has been shown that it is possible to focus acoustic energy with PCs through negative refraction [12,13]. It is also possible to stack PCs with different filling fractions to make a Gradient Index (GRIN) lens [13–17] for sound focusing. AMMs usually contain an array of resonators of sub-wavelength size, and have been used to focus ultrasound via hyperbolic planar lenses [18] or space coiling [19–21]. Other options to focus sound include fractal AMMs [22,23], metasurfaces [24], Luneburg lenses [25], polymer cuboids [26], "+" shaped steel rods PCs [27] exagonally-arranged PCs [28], and polyurethane-based ball lens [29], to mention some.

It has been demonstrated that planar polymer lenses can be additively-manufactured to achieve extraordinary transmission in air [11]. It must be stressed that in such lenses, the lens focusing was boosted by Fabry-Pérot (FP) resonances generated in the air channels between the polymer lens rings. Due to the large acoustic impedance (Z) difference between air and polymer, sound transmitted in the air channels can generate FP resonances in the form of standing waves, helping to amplify the intensity at the focal region at a specific frequency, i.e. at the FP resonant condition. Further, little energy is transmitted into the solid material due to the large impedance mismatch that exists.

However, the Z value of standard polymers is close to that of the water. Hence, sound energy would not be well-confined within any water channels as energy could enter into the polymer, altering the intended behaviour. Therefore, metal-based lenses are commonly employed to achieve focusing in water — the interested reader can refer

* Corresponding author.
E-mail address: stefano.laureti@unical.it (S. Laureti).

https://doi.org/10.1016/j.ultras.2022.106781
Received 28 October 2021; Received in revised form 10 May 2022; Accepted 31 May 2022
Available online 3 June 2022

to e.g. Fuster et al. [30], or to Pérez-López et al. [31] for detail of such lenses. However, being able to manufacture and use polymer-based acoustic lenses for use in water would be of high importance for e.g. medical treatment, especially when therapeutic ultrasound is used in combination with electromagnetic monitoring and imaging techniques such as magnetic resonance imaging (MRI), as polymer devices do not interfere with the magnetic field [32,33].

An attempt to circumvent the mentioned impedance issue can be found in [34], where polymer-based reversal Fresnel zone plates lenses have been successfully manufactured to focus ultrasound in water. Zone plate lenses can be tuned to have a variable focal patterns to minimize sidelobes and maximise gain [35]: the possibility to change the focus is of particular interest for medical applications. Rubber foam has also been demonstrated to be an effective medium for manufacturing such lenses, as randomly-enclosed air bubbles within the foam enhance the impedance mismatch with the surrounding water [36].

Recently, a "trapped-air" concept has been introduced by Terrazó-Serrano et al. for realizing PLA-based planar lenses [32], and by Laureti et al. [39] to design polymer-based holey-structured AMMs, both for use in water. In [32], it was shown that trapping air within a polymer shell is a good strategy for enhancing the overall impedance mismatch with the surrounding water. Hence, a polymer-based planar lens having an opaque central area was successfully realised and its focussing capabilities were compared against different polymer and brass counterparts. The results showed that such an approach leads to an efficient focussing in water at 250 kHz, although achieving lower intensity when compared to a brass lens. In [39], a polymer-based structure was realised by trapping an air layer within a polymeric shell, which can be used for sub-wavelength imaging in water at close range using evanescent waves coupling through FP resonances. This trapped-air device was realised using commercial additive manufacturing equipment and it was shown to achieve a better performance than its metallic counterpart in terms of imaging, this being the result of the high impedance mismatch provided by the air volume trapped within the polymer shell with the added benefit of using the FP resonances to improve the focussing performances.

The trapped-air and FP concepts are exploited here for optimal focussing in water via a concentric ring geometry. With respect to the state-of-the-art [32], the present lens exploits the following additional strategies:

1) A polymer-based trapped-air planar lens having transparent central zone is both simulated and tested experimentally. This choice is shown to provide a higher intensity in the focal region when compared to a design where there is no transmission in this region of the lens, especially important for a lens with relatively-low number of channels, see [31];
2) Given that the intended working frequency of the trapped-air lens was 500 kHz, the lens geometry is calculated via the well-known constructive interference formula (see Eq.1). In addition, the thickness of the trapped-air lens is chosen such that the FP resonant condition within the concentric transmission channels is at the same frequency of 500 kHz. This design would be expected to give an enhanced performance when compared to lenses that do not employ this additional FP resonance. Thus the transmission coefficient of the lens is maximized at such frequency, see [11,37]. This results in an improved focussing performance when compared to a lens with a random choice of the lens thickness;
3) The effect of different polymer wall thicknesses used to construct the trapped air structures on the intended lens behaviour is explored, both numerically and experimentally, to give a comprehensive view of the additive-manufacturing parameters that have to be considered when fabricating such trapped-air devices.

To illustrate the benefit of the proposed approach, trapped-air lenses having both a non-optimal thickness (i.e. that would not result in a FP resonance) and one where the FP resonance matches the Fresnel zone design frequency are compared. A comparison with a metal-based counterpart is also shown.

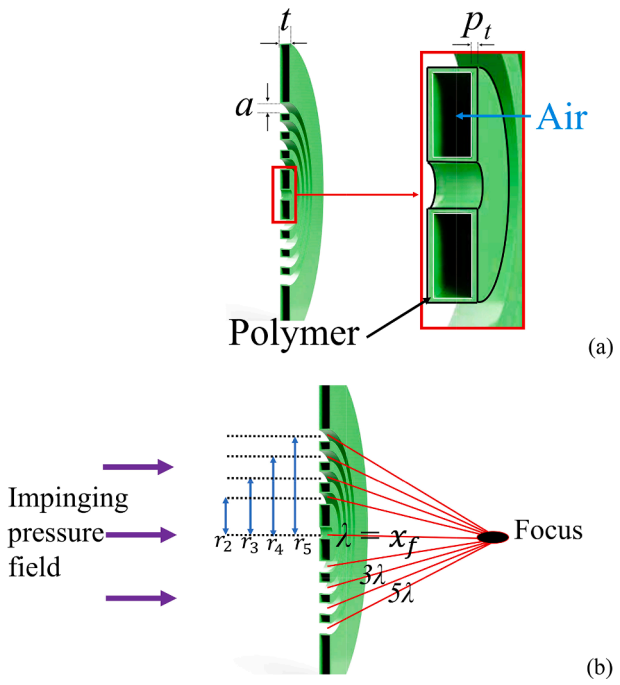

Fig. 1. (a) Cross sections of a trapped-air lens. The inset to the right is an expanded view of the central trapped-air channel. (b) An illustration of an incident planar pressure wave being focused by the lens at a focal distance x_f which is equal to one wavelength (λ).

2. Polymer trapped-air lenses

Schematic diagrams of a trapped-air lens is shown in Fig. 1(a) and (b) to highlight the main geometric variables employed in the design. Here, t is the lens thickness, a is the width of the channels and p_t is the polymer thickness chosen to trap the air volume. If the rings are placed strategically, they allow sound to be focused, regardless of the lens thickness.

In this work, the focal point is arbitrarily chosen to be at a distance $x_f = \lambda$ from the lens outlet, meaning that the acoustic signal transmitted through adjacent straight water-filled channels will constructively interfere if the distance from each channel outlet to the chosen focal point is a multiple of λ, as shown in Fig. 1(b). The distance between adjacent radii (r_i) (for $r_2 - r_5$) can be calculated using Eq. (1) [11], noting that r_1 is zero:

$$r_i = \sqrt{\left(\lambda + \sqrt{x_f^2 + r_{i-1}^2}\right)^2 - x_f^2} = \lambda\sqrt{(i^2-1)} \qquad (for\ x_f = \lambda) \tag{1}$$

The focal distance was chosen to be equal to a wavelength because there is a trade-off between the number of water channels diffracting sound and the focal distance. More channels allow for a better constructive interference, but a spacing is required between them, as shown in Eq. (1). As the transducer employed in the experiment had a diameter of 22 mm, it was decided to aim for at least 5 diffracting channels fully within the incident ultrasonic beam, hence the choice of $x_f = \lambda$.

As mentioned in Section 1, the current design exploits the fact that the thickness of the lens can be used to select a specific frequency/wavelength at which the intended lens design works best via the FP resonance mechanism within the water channels. Thus, the focal point amplification can be boosted by FP resonances generated in the water-filled channels [10]. This represents an advantage because a large fraction of the incident pressure wave is reflected by the trapped-air

Table 1
Values of speed of sound, shear-wave speed, density and acoustic impedance for air, water and PLA polymer.

Material	c_P = speed of sound (pressure-wave speed) [m•s^{-1}]	c_L = shear-wave speed [m•s^{-1}]	ρ = Density [kg•m^{-3}]	Z = Acoustic impedance [kg•s^{-1}•m^{-2}]	Z/Z_{air}	Z/Z_{water}
Air	343	–	1.2	411.6	1	$0.27•10^{-3}$
Water	1,480	–	1,000	$1.48•10^{6}$	$3.6•10^{3}$	1
PLA	1,860	980	1,240	$2.3•10^{6}$	$5.6•10^{3}$	1.56

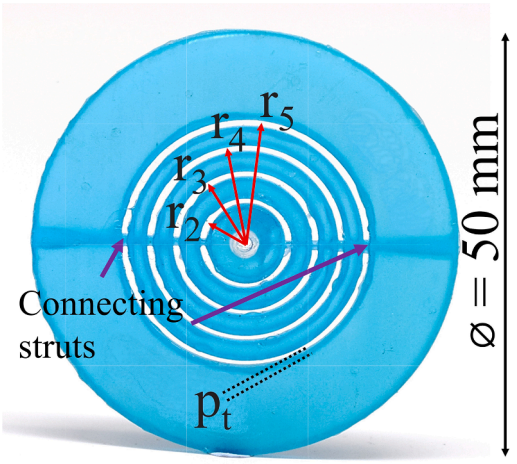

Fig. 2. A photograph of a typical trapped-air lens.

zones. FP resonances are mainly regulated by the lens overall thickness t, which is the length of the water-filled channels. FP resonances are expected at integer multiples of the fundamental frequency f_1, and can be calculated as:

$$f_1 = \frac{1}{2}\frac{c}{t} \tag{2}$$

where $c = 1480$ m•s^{-1} is the speed of sound in water at room temperature [38]. Choosing a thickness $t = 1.48$ mm, the first resonance in frequency is expected at $f_1 = 500$ kHz where $\lambda = 2.96$ mm. By fixing the focal point x_f at one wavelength distance (2.96 mm), using Eq. (1), the channel radii values are obtained: $r_1 = 0$ mm, $r_2 = 5.13$ mm, $r_3 = 8.37$ mm, $r_4 = 11.46$ mm and $r_5 = 14.5$ mm.

The lens was thus designed to focus the incoming wave at a distance of 2.96 mm from the middle channel at 500 kHz, provided that the acoustic impedance mismatch between the lens material and the surrounding medium is sufficiently large, i.e. provided that the trapped-air rings stop a good portion of the impinging pressure. The choice of the lens thickness $t = 1.48$ mm is such that the FP resonant mechanism happens at the same frequency for which the lens has been designed, i.e. at 500 kHz. Thus, the hybrid lens design provides a maximized transmission coefficient at 500 kHz, as shown by Moléron et al. [11] in air, and by Laureti et al. for holey-structured metamaterials in water [39].

As stated earlier, a wide range of suitable materials for developing the intended acoustic lens would be available for use in air, including polymers such as polylactic acid (PLA), as the acoustic impedance (Z) mismatch with air is around three orders of magnitude, see Table 1. However, polymers and water have similar Z, hence the choice of trapping air. Note that the reported values for PLA are good representatives for the whole class of polymers. In addition, the sound velocity used for PLA is in line with what reported in Agu et al. [40]. This value is lower than the value of of 2,220 m•s^{-1} that is usually assumed for bulk material, but is more representative of the PLA when additively-manufactured, especially when potential voids and imperfect/uneven curing process may reduce the speed of sound.

The trapped-air polymer lenses were fabricated using micro-stereolithography, an additive manufacturing technique, using a Formlabs Form 2 printer (Somerville, Massachusetts, United States), and a V5T resin. The geometry was sliced and fabricated into 50 μm thick layers. Lenses were initially manufactured in one fabrication operation, noting that the need for internal cavities that did not link one wall to another meant that internal supports could not be used. Additionally, as the lens was submerged in resin during the build, excess resin needed to be drained through small holes included within the structure. Due to these two issues, the lenses collapsed inwards during printing and curing. It was therefore decided to separate each lens into a 'body' and 'lid', with adhesive used to combine the two halves as a post-process

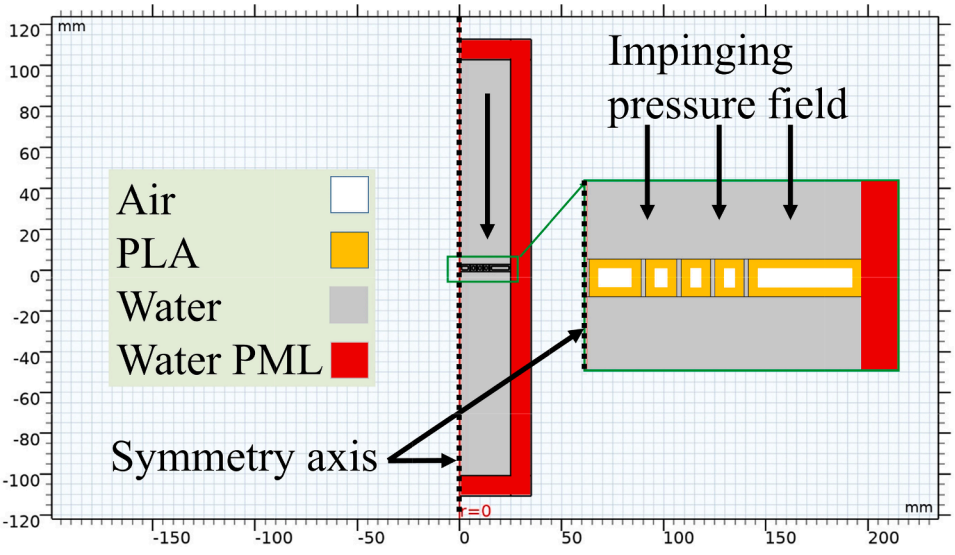

Fig. 3. 2D axisymmetric COMSOL Multiphysics® model sketch employed to assess the lenses amplification. The inset shows an expanded view of the lens.

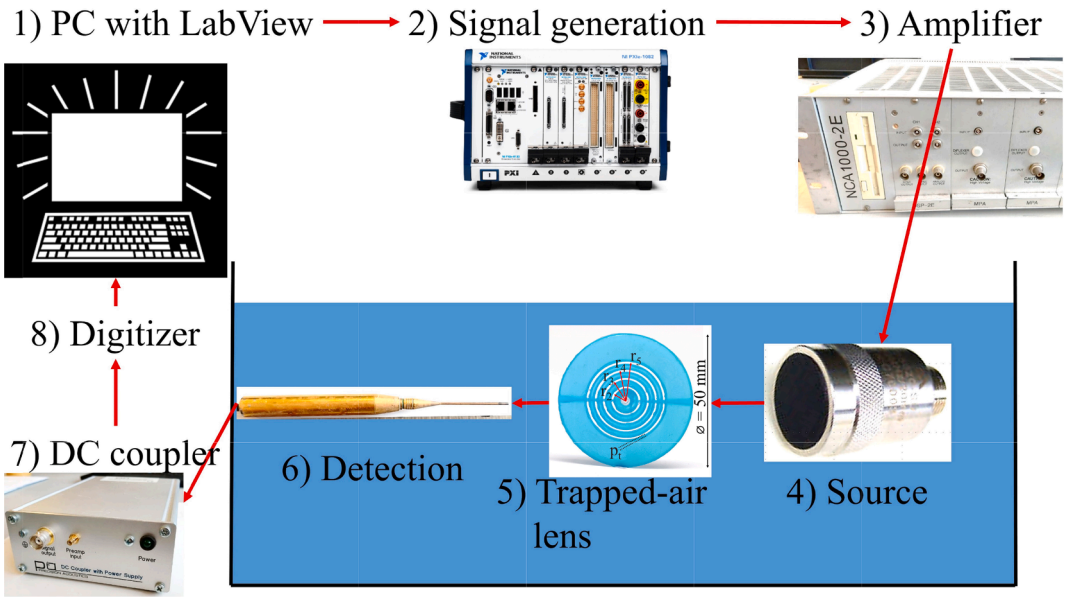

Fig. 4. A sketch of the experimental setup. A PC (1) manages both the signal generation/acquisition and synchronisation through a routine in LabVIEW environment. The generated signal is sent to a National Instrument PXI-5421 digitiser (2) and amplified by a NCA 1000-2E (3). A custom-made transducer (4) emits the acoustic field in water impinging over the trapped-air lens (5). The detection is carried out (6–7) via a Precision Acoustic hydrophone that senses the scattered field and it is moved via a motorized 3-axis stage. The acquired signal is digitised via a National Instrument PXI-5122 (8) at 100 Msamples/second before being transferred to the PC.

operation, sealing the air channels. Parts were printed at an angle of 45° with respect to the printer bed, with external supports added manually in FormLabs PreForm software. To connect the trapped-air rings, small struts were employed, as shown in [11]. These slightly reduced the overall constructive interference but were needed to achieve the concentric design. The reader is referred to [41] for further insights on the micro-stereolithography manufacturing process. An example of trapped-air lens built using this technique is shown in Fig. 2.

3. FEM and experiments on trapped-air lenses

3.1. Simulations

Several comparisons between FEM simulations of trapped-air lenses and experiments were conducted. In the models, air volumes were trapped within a PLA shell of variable polymer thickness p_t of 0.4 mm, 0.6 mm, and 0.8 mm. A 2D FEM Axisymmetric Frequency Domain model was built in COMSOL Multiphysics (Stockholm, Sweden), which considered the Acoustic-Solid interaction for the PLA shell to verify and compare the sound focusing effect of such lenses. To this aim, both the c_p and c_L were specified for the PLA to consider mode conversion occurring in the solid material. Moreover, the "Fixed Constraint" conditions have been applied to the on-axis (vertical) boundaries of the lens so as to mimic the presence of the struts connecting the rings, which would be freely vibrating with the employed 2D modelling otherwise.

Each lens was made by revolving six rectangular sections, creating five water channels between them, around an axis of symmetry. Before and after the lens, two water control volumes were used to simulate propagation in water, and the whole geometry was surrounded by a Perfectly Matched Layer (PML) to simulate anechoic conditions so as to avoid reflections. Material properties used for the model are listed in Table 1. A planar background pressure field of 1 Pascal amplitude was applied parallel to the vertical axis (from top to bottom) to simulate a travelling plane wave incident upon the lens. The frequency range studied was 400–600 kHz, as these lenses were designed to focus at 2.96 mm distance from the lens at the fundamental frequency $f_1 = 500$ kHz. The model is shown Fig. 3:

A space-varying mesh was applied to ensure there were at least 10 elements per wavelength at the smallest dimension, which in this model was the polymer thickness p_t (coloured orange in Fig. 3). For fabrication reasons, the channel aperture a (which is the separation between adjacent lens channels) has to be greater than twice the polymer thickness p_t, otherwise there would not be space between the lens rings. p_t values of 0.4, 0.6 and 0.8 mm, which are near the lower resolution limit of the available stereolithography equipment, were investigated, and this led to a channel aperture choice of $a = 2$ mm (the channel aperture is effectively the water channel width plus twice the polymer thickness used to enclose the air volumes). A water channel length (which is also the lens thickness) value of 1.48 mm was used to obtain the correct FP resonant frequencies for boosting the focusing effect, as described above.

3.2. Experiments

Experiments were performed using an unwindowed chirp signal of 75 μs duration, sweeping from 300 to 700 kHz as a signal to drive an ultrasonic transducer in a custom-made water tank. The signal was generated using a National Instruments PXI-5421 waveform generator which was amplified using an NCA 1000-2E amplifier and used to drive a 500 kHz piezocomposite custom-made ultrasonic transducer (Cambridge Tech Ltd, Cambridge, UK) with an active diameter of 22 mm. The signal travelled through the water to the lens, which was positioned on-axis at a distance of 150 mm from the source. The resulting pressure field produced by the lens was detected by a scanned 0.5 mm diameter Precision Acoustic hydrophone via a PC-controlled motorized 3-axis stage. The hydrophone was used to acquire the transmitted acoustic waveform across a 10 × 10 mm horizontal plane, which was then recorded using a National Instruments PXI-5122 Digitizer at a sampling rate of 100 Msamples/second. The recorded signals were post-processed using a Chirp Z-transform (CZT). The CZT was chosen for its flexibility: after entering sampling rate and signal length, it was possible to adjust the frequency resolution and the number of output points. In these experiments, the frequency components were assessed at 100 Hz steps. More insight on the CZT can be found in [42]. This allowed the response of the lens to be analysed at frequencies between 300 and 700 kHz. The experimental results were then normalised relative to the field that

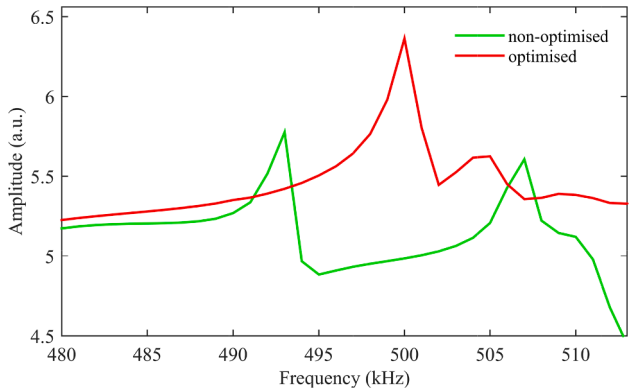

Fig. 5. FEM predicted amplitudes at the focal point for the optimised (t = 1.48 mm) and non-optimised (t = 1.5 mm) trapped-air lenses.

existed with no lens in place, so that the effect of the lens could be more effectively studied. A sketch of the experimental setup is shown in Fig. 4:

4. Results

The results are shown in each case for the resultant pressure field as a function of the axial distance for frequencies between 400 and 600 kHz. The pressure field in both FEM and experiments was normalised using water as a baseline reference so to obtain normalised values (referred to here as amplification).

With the help of FEM, it was found that matching the FP frequency to the lens geometry was an important factor. The optimum design was expected when the FP resonance exactly matched the frequency used to design the zone structure of the lens (500 kHz and a lens thickness of $t =$ 1.48 mm). This was compared to a lens with the same overall design but with a slightly increased non-optimum lens thickness of $t = 1.50$ mm, where the resonance would be expected at 493 kHz. Fig. 5 plots the

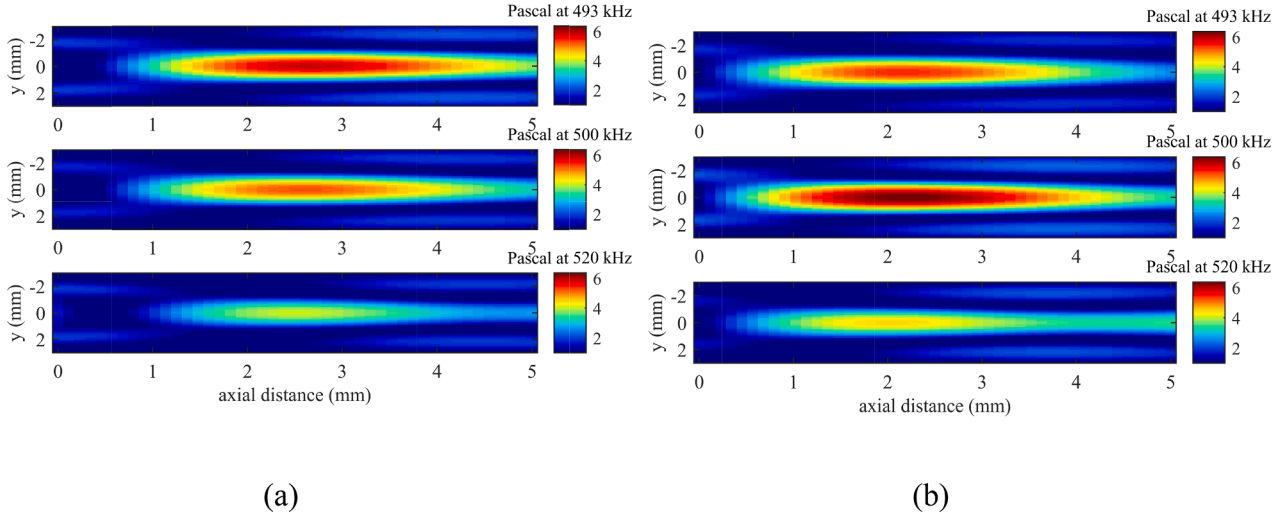

Fig. 6. (a) Predicted FEM amplification at 493 kHz, 500 kHz and 520 kHz at different distances from the lens outlet, for the non-optimised trapped-air lens design. (b) Same as (a), but for the optimised case.

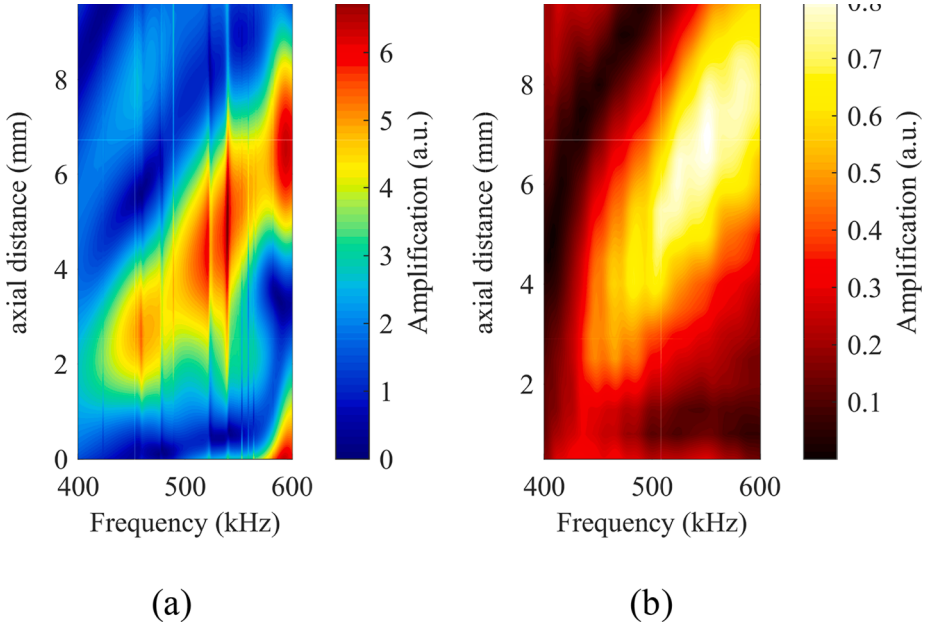

Fig. 7. (a) FEM prediction and (b) experimental results for the pressure field at various axial distances as a function of frequency. The results are shown for distance along the lens axis for a trapped-air lens with $p_t = 0.4$ mm.

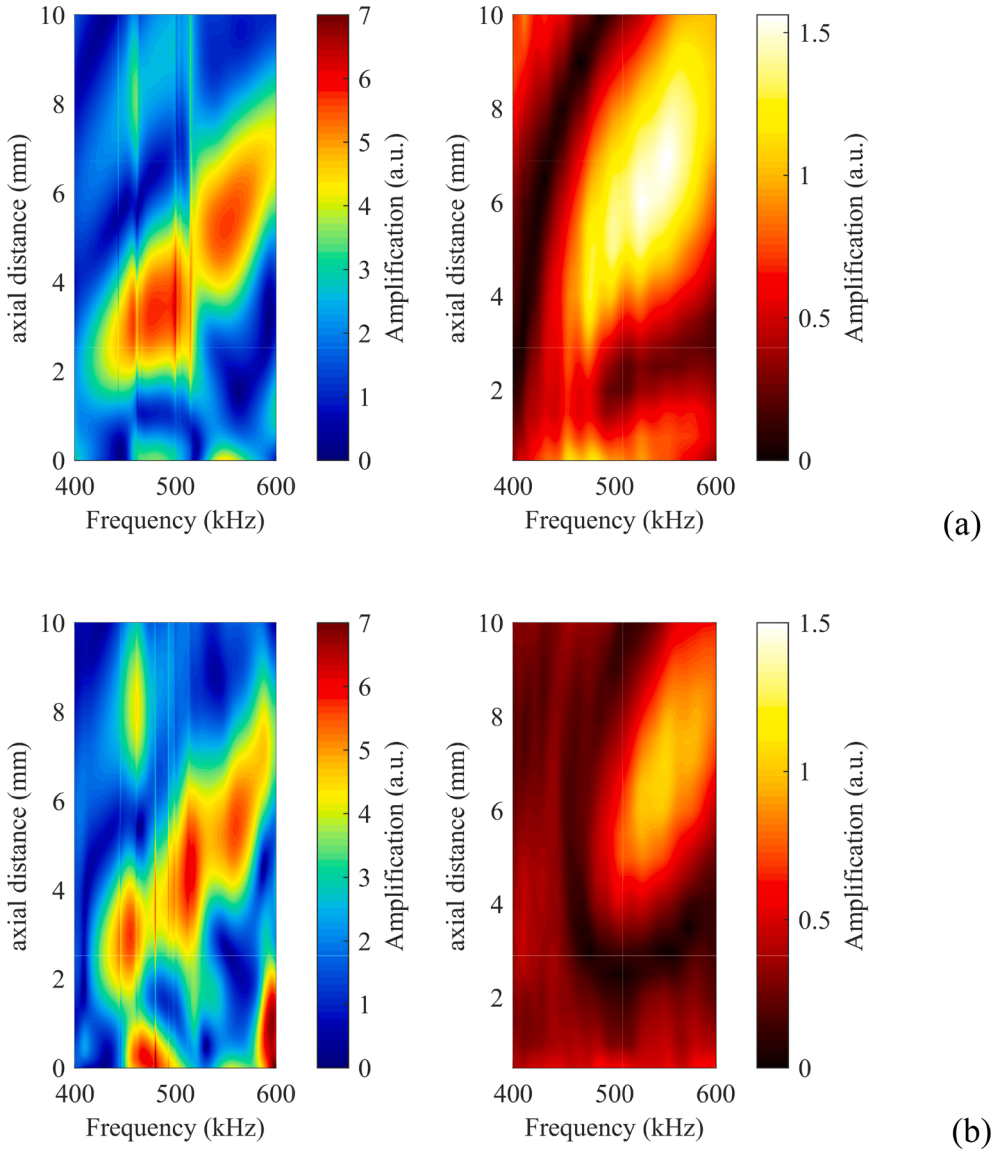

Fig. 8. FEM predictions (left) compared to experimental results (right) of the pressure field as a function of the axial distance for multiple frequencies on two trapped air lenses with (a) $p_t = 0.6$ mm and (b) $p_t = 0.8$ mm.

expected amplitude at the focal point for both designs over the 480–515 kHz frequency range. It is evident that a single peak response at the required frequency is obtained for the optimum frequency/lens geometry combination, whereas response at the lower non-optimised frequency shows a double peak and lower amplitude. This demonstrates that the choice of the lens thickness is crucial for ensuring that the FP effect occurs at the intended working frequency of the lens, i.e. at 500 kHz, and this shows the difference to previous papers where a FP resonance was not included.

Further insight can be gained by looking at the spatial variations across the focal regions for each design at three selected frequencies of 493 kHz, 500 kHz, and 520 kHz. The resulting predictions are shown in Fig. 6, where it can be seen that the best response is predicted at 500 kHz for the optimised design, where the FP resonance coincided exactly with the designed lateral lens geometry, showing the importance of the FP resonance in enhancing the response. Thus, every lens described subsequently has been constructed with an optimal thickness of $t = 1.48$ mm.

Fig. 7(a) shows numerical predictions of a trapped-air lens surrounded by a polymer layer of thickness $p_t = 0.4$ mm, which can be compared to experimental results in Fig. 7(b).

The trend predicted by the model matches the experimental one. In both cases, the focal point shifts in distance with frequency, which is as expected for such a lenses. The model predicts an amplification that is higher in value than the experiment: this difference is thought to be mainly due to the model being frictionless, with no losses, whereas a viscoelastic polymer was used to form the solid shell. Note that the upper limit of the amplification in the model was set to 7, even though some resonances could reach higher values, this was done so as to highlight the acoustic response of the lens and was kept consistent in all the models.

The model predicted resonances based on the vertical high amplitude lines in Fig. 7, which are thought to be due to FP resonances, as they are of narrow bandwidth at particular frequencies. It is expected that such resonances would be mainly generated in the water channels, but it is possible that coupling into the trapped-air structure could introduce resonances in the trapped air volumes or the polymer shell. Such resonances are also seen in the experiment, but at slightly different frequencies. This is probably due to the model being ideal, whereas the actual lens will have natural variations in structure due to the fabrication process.

Note that the expected focus is not at 2.96 mm at 500 kHz, as

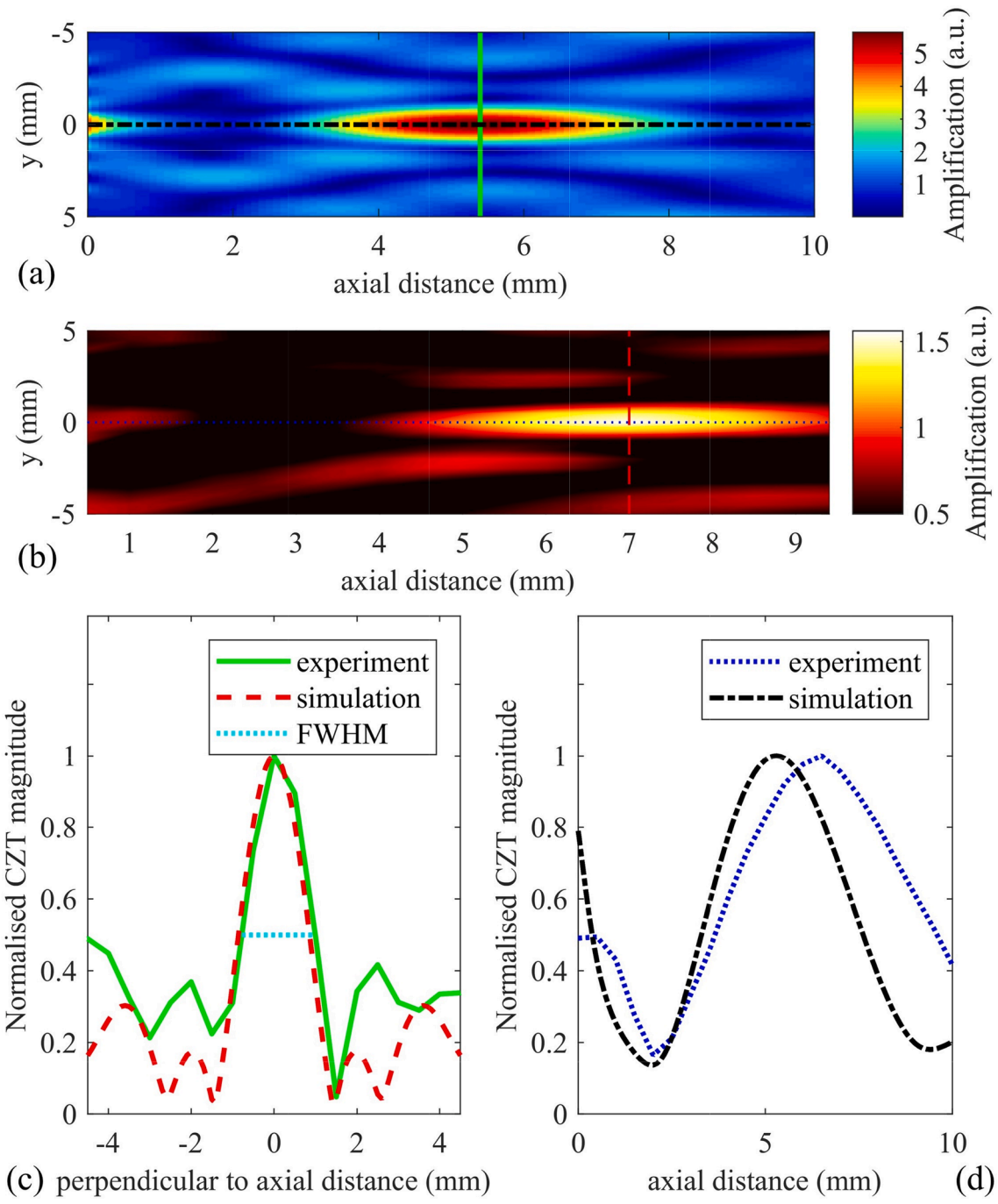

Fig. 9. (a) Amplification in the focal region predicted via the FEM design at 551.3 kHz. (b) As in (a) but experimentally-measured using the scanned hydrophone at 551.3 kHz. (c) and (d): the variation in amplitude along the two lines in Fig. 9(a) and (b), namely perpendicular and parallel to the axis distance, for both FEM and experimental results. The cyan dashed line shows the position at which the FWHM was estimated from the data.

designed, due to the interaction between trapped-air channels and the water-filled ones. The channels were not ideal for resonance generation due to their low aspect ratio t/a – which is only $1.48/2 = 0.74$, and this likely has an effect on the resonant frequencies. Despite blocking a good part of the sound, the amplification is almost 1 and there is a focal region which could be useful for imaging as it has more amplitude than the background. The differences between the focal position measured experimentally and the focal position predicted using FEM is thought to be related to manufacturing imperfections which occurred during the micro-stereolithography fabrication process. This involved manufacturing the lens from two separate parts which were then joined together. This is bound to introduce some variability in the operation of the final lens construction which are difficult to quantify.

Fig. 8(a) and (b) show the result of changing the polymer thickness p_t to 0.6 mm and 0.8 mm.

Again, the trend of the model is confirmed experimentally, but this time the trapped-air lenses are shown to amplify the pressure field in the region of the focus experimentally (i.e. > 1 with respect to the response without the lens present). This is despite the reduction of the channel width caused by the increase in polymer shell thickness p_t. Note that the effective width of the water channel would be 0.8 mm in the 0.6 mm p_t case and 0.4 mm in the 0.8 mm p_t case; this is because $a = 2$ mm. Such enhancement of the amplitude at the focus is thus thought to be due to stronger FP resonances in the water channels. The aspect ratio (t/a) of

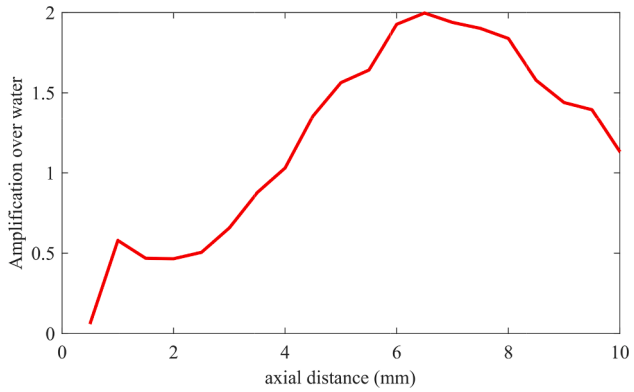

Fig. 10. Amplification along the focal axis obtained with a 21 cycle tone-burst at 551.3 kHz.

the water channels in these two cases were 1.85 for the 0.8 mm wide channels and 3.7 for the 0.4 mm wide channels. The higher the aspect ratio, the stronger the FP resonance expected. From the above, we can conclude that additively-manufactured trapped-air polymer lenses are focusing ultrasound in water and could be therefore a valid and cheaper replacement to additively-manufactured metal lenses.

A parameter of interest for lenses is the spatial extent of the focal region. This can be estimated via the Full Width at Half Maximum (FWHM) value, calculated along a line through the focal region and perpendicular to the propagation axis. The FWHM is defined as the distance between two locations along the axis of measurement which are at half the maximum amplitude, and can be used to estimate the achievable resolution for a given frequency. In the case of the 0.6 mm p_t trapped-air lens, the FWHM was 0.65 λ, where λ at this frequency is 2.69 mm in water. Fig. 9(a) shows the focus predicted at 551.3 kHz using FEM, whilst Fig. 9(b) shows the experimental results at the same frequency, i.e. the frequency value at which the measured was the highest. In addition, Fig. 9(c) and (d) display the intensity of the normalised CZT magnitudes in directions both parallel (the length of focal zone) and perpendicular (the beam diameter at the focus) to the focal axis respectively. Good agreement is found between FEM prediction and experimental results. Note that the plotted fields were normalised to their respective maxima so as to more clearly estimate the FWHM values.

In diffraction-limited lenses, the value of the FWHM cannot be below 0.5 λ. The closer the FWHM is to 0.5 λ, the better the lens, because the resolution increases. One way to surpass this limit and obtain a lens with a FWHM below 0.5 λ is to use a superlens, based on the use of negative

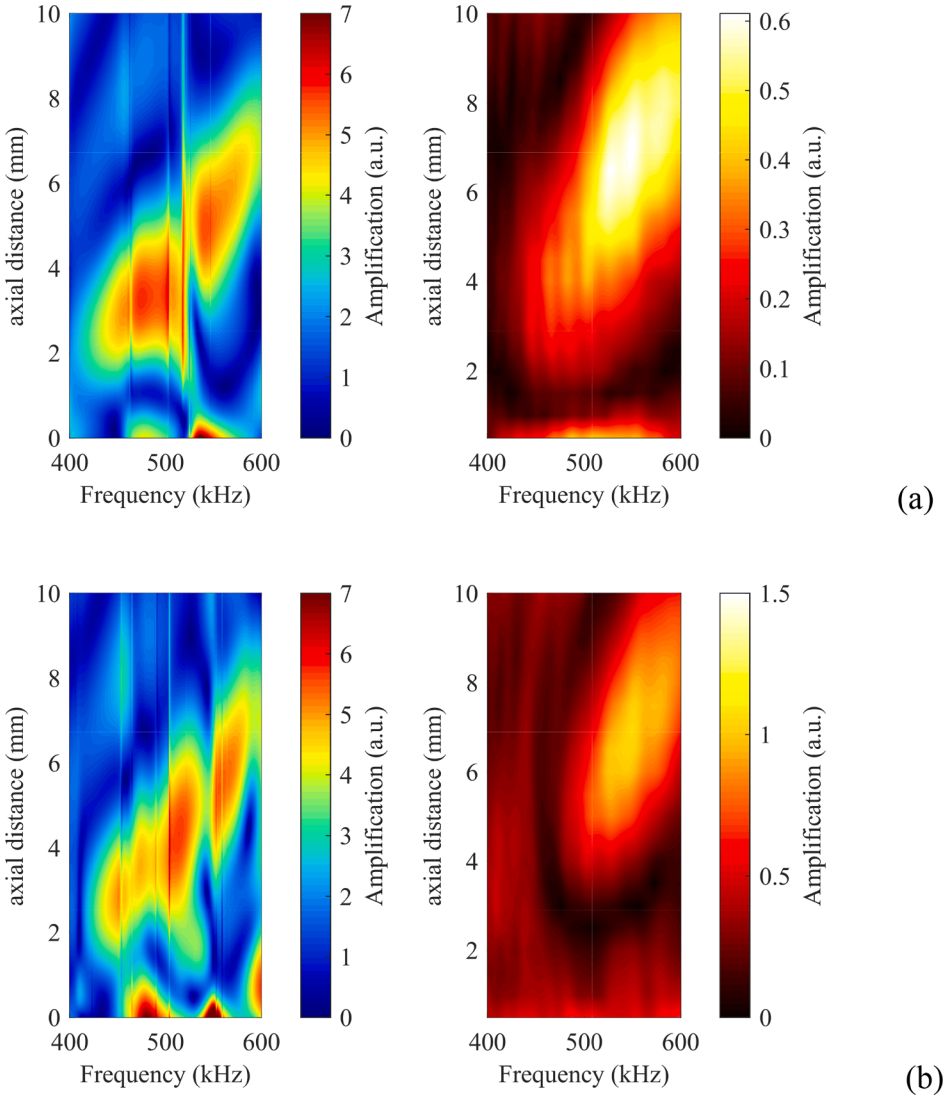

Fig. 11. (Left) FEM predictions and (right) experimental results of the pressure field as a function of the axial distance for multiple frequencies for a trapped-air lens with (a)$p_t = 0.6$ mm and (b) $p_t = 0.8$ mm with doubled lens thickness.

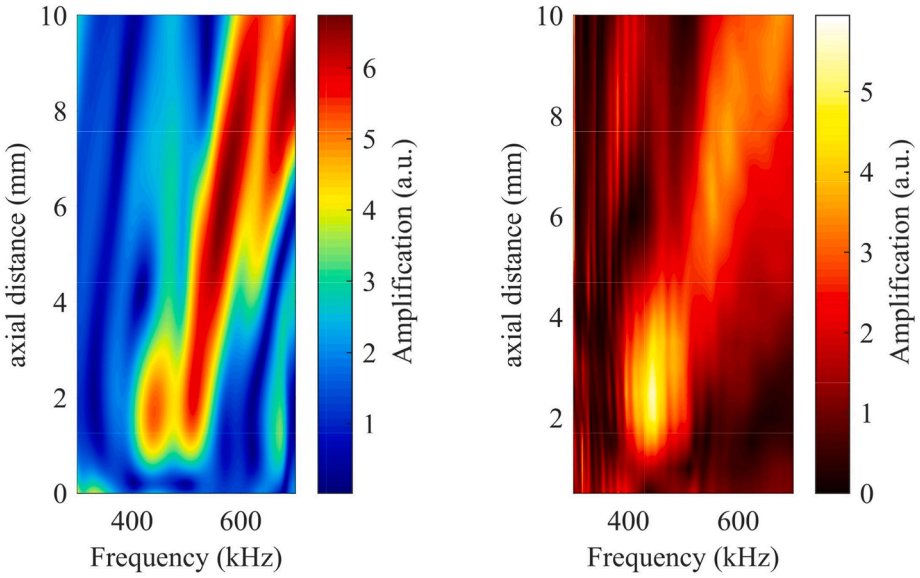

Fig. 12. (Left) FEM predictions and (right) experimental results of the pressure field as a function of the axial distance for multiple frequencies, for a brass lens with optimised thickness.

index media [43]. Conversely, the trapped-air lenses here discussed are diffraction-limited since the focusing principle relies on standard diffraction theory, but an experimental value of 0.65 λ is a resolution comparable to lenses shown in other work using Fresnel-type lenses and resonances [11].

A further experiment was carried out to investigate the effect of the input signal on the focusing amplification. When repeating the experiment using a 21 cycle tone-burst with the same 0.6 mm p_t lens at 551.3 kHz, it was found that an even higher amplification could be obtained, as shown in Fig. 10.

The maximum measured amplification within the focal region using the 21 cycle tone-burst was 2, while with the chirp it was only 1.65. This difference is due to the chirp distributing its power at multiple frequencies, so there is less power at a specific frequency. In addition, a tone-burst allows more time for a resonance to build up within the water-filled channels, and this has a beneficial effect on the maximum amplitude at the focus.

The effect of doubling the overall thickness (t) of the lens was also investigated so that the effect of using a different FP resonant harmonics on the focal point could be assessed. Fig. 11(a) and 11(b) show a comparison similar to that shown earlier in Fig. 8(a), but now with a thickness of $t = 2.96$ mm instead of 1.48 mm. This resulted in the first FP harmonic being at 250 kHz and the second one at 500 kHz. The thickness t is of importance for two reasons: it changes the harmonics present for the FP resonance (which in the case of the water channels was the 1st harmonic with $t = 1.48$ mm and the 2nd when $t = 2.96$ mm) and the aspect ratio (t/a) of the water channels. FP resonances usually benefit from a high aspect ratio, but there is a trade-off to consider with respect to fabrication, in that thin walls are more difficult to make, especially when fabricating sub-mm thicknesses devices.

It can be seen from Fig. 11 that doubling the lens thickness had a detrimental effect on the intensity at the focus, but it still demonstrated a lens effect as the intensity at the focus was greater than the background level.

As a final comparison, the focusing capabilities of a brass lens having both the same optimised thickness $t = 1.48$ mm and radii of the optimised trapped-air lens are shown in Fig. 12:

It can be seen that the metal lens produced a higher amplification than the trapped-air lenses, both in simulation and experimentally. In addition, the measured amplification values are closer to the FEM values than for the trapped-air case. Again, this is thought to be due to sound penetrating into the polymer layer, changing in turn the expected behaviour of the trapped-air lens with respect to the metal counterpart.

5. Conclusions

Additively-manufactured lenses made of trapped-air rings separated by water channels were designed to focus ultrasound in water. Both numerical predictions and experimental results confirmed that an enhanced focus could be obtained by selecting the correct lens thickness for achieving FP resonances. An advantage of these lenses is that the trapped-air design creates an extremely high acoustic impedance mismatch with water, even though the solid structure was fabricated from polymer material. This enabled the generation of Fabry-Pérot resonances in the water-filled channels. The lens can be used in the same way as any other ultrasonic lens to be used in water, as it is totally waterproof with a robust design.

The Fabry-Pérot resonance is a narrow bandwidth effect, which occurs at a specific frequency and at integer multiples of it. This means that it is difficult to extend this beneficial effect to a wider range of frequencies using the current design. However, a good strategy for dealing with this was proposed for use in air in Ref. [11], where meandering channels were added to extend the frequency range. Another approach might be to vary the thickness across the build. These approaches will be the object of future work.

There are some advantages to the proposed design. The first of these is that the micro-stereolithography fabrication method used here can be employed for more complex geometries based on a polymer material. Thus, further developments (e.g. varying the thickness across the lens, including curved channels etc) is much more difficult in a metallic lens that cannot use this fabrication method. Another advantage is that the trapped-air lenses are flat (unlike a Fresnel lens), and could for example be placed against a skin surface for biomedical imaging. The approach thus combines the advantages of both Fresnel lenses and flat metallic designs that do not include a FP resonance in their design. Despite metal being able to focus more energy into the focal region, for some medical procedures it is not possible to use metallic components. An example is when ultrasonic imaging is used in conjunction with MRI imaging. There is also a strong difference in cost when printing metals particles or using stereolithography. Thus, in these cases polymer lenses may be preferred.

Trapping air to make a lens has thus been shown to be a promising technique for ultrasound imaging and sensing applications. Future work

will focus on extending the Fabry-Pérot effect to a broader range of frequencies, e.g. realising a variable-thickness trapped-air lens to combine multiple beneficial resonance effects.

CRediT authorship contribution statement

Lorenzo Astolfi: Methodology, Data curation, Formal analysis, Investigation, Software, Validation, Visualization, Writing – original draft, Writing – review and editing. **David A. Hutchins:** Project administration, Funding acquisition, supervision, Methodology, Data curation, Formal analysis, Investigation, Validation, Visualization, Writing – original draft, Writing – review and editing. **Richard L. Watson:** Formal analysis, Validation, Visualization, Writing – review and editing. **Peter J. Thomas:** Funding acquisition, Supervision, Writing – original draft, Formal analysis, Validation, Visualization, Writing – review and editing. **Marco Ricci:** Methodology, Funding acquisition, Supervision, Methodology, Data curation, Formal analysis, Investigation, Validation, Visualization, Writing – original draft, Writing – review and editing. **Luzhen Nie:** Data visualisation, Investigation, Writing – review and editing. **Steven Freear:** Project administration, Funding acquisition, Supervision, Validation, Writing – review and editing. **Timothy P. Cooper:** Data visualisation, Investigation, Writing – review and editing. **Adam T. Clare:** Project administration, Funding acquisition, Supervision, Validation, Writing – review and editing. **Stefano Laureti:** Conceptualisation, Software, Project administration, Funding acquisition, Supervision, Methodology, Data curation, Formal analysis, Investigation, Validation, Visualization, Writing – original draft, Writing – review and editing.

Declaration of Competing Interest

The authors declare that they have no known competing financial interests or personal relationships that could have appeared to influence the work reported in this paper.

Acknowledgements

Funding for this work was provided through the UK Engineering and Physical Sciences Research Council (EPSRC), Grant Numbers EP/N034163/1, EP/N034201/1 and EP/N034813/1. Dr. Stefano Laureti acknowledges the financial support from Programma Operazione Nazionale e Innovazione 2014-2020, Fondo Sociale Europeo, Azione 1.2 “Attrazione e Mobilitá Internazionale dei Ricercatori” - CUP: H24I19000410005.

References

[1] C.M.C. Tempany, E.A. Stewart, N. McDannold, B.J. Quade, F.A. Jolesz, K. Hynynen, MR imaging-guided focused ultrasound surgery of uterine leiomyomas: a feasibility study, Radiology 226 (2003) 897–905, https://doi.org/10.1148/radiol.2271020395.

[2] D. Jeanmonod, B. Werner, A. Morel, L. Michels, E. Zadicario, G. Schiff, E. Martin, Transcranial magnetic resonance imaging-guided focused ultrasound: noninvasive central lateral thalamotomy for chronic neuropathic pain, Neurosurg. Focus. 32 (1) (2012) E1.

[3] N. McDannold, G.T. Clement, P. Black, F. Jolesz, K. Hynynen, Transcranial magnetic resonance imaging- guided focused ultrasound surgery of brain tumors: Initial findings in 3 patients, Neurosurgery. 66 (2010) 323–332, https://doi.org/10.1227/01.NEU.0000360379.95800.2F.

[4] T.-H. Gan, D.A. Hutchins, D.R. Billson, D.W. Schindel, High-resolution, air-coupled ultrasonic imaging of thin materials, IEEE Trans. Ultrason. Ferroelectr. Freq. Control. 50 (11) (2003) 1516–1524.

[5] X. Jiang, K. Snook, W.S. Hackenberger, X. Geng, Single crystal piezoelectric composites for advanced NDT ultrasound, Nondestruct, Charact. Compos. Mater. Aerosp. Eng. Civ. Infrastructure, Homel. Secur. 2007 (6531) (2007) 65310F, https://doi.org/10.1117/12.715150.

[6] Y. Liu, H. Zhang, J. Yang, X. Zhang, S.-y. Zhang, L.i. Fan, G. Gu, Sound regulation of coupled Helmholtz and Fabry-Pérot resonances in labyrinth cavity structures, Ultrasonics 95 (2019) 45–51.

[7] M. Fink, Ultrasonic Time Reversal Mirrors, J. Phys. D. Appl. Phys. 26 (9) (1993) 1333–1350.

[8] O.T. Von Ramm, F.L. Thurstone, Cardiac imaging using a phased array ultrasound system. I. System design, Circulation 53 (1976) 258–262, https://doi.org/10.1161/01.CIR.53.2.258.

[9] R.O. Illing, J.E. Kennedy, F. Wu, G.R. Ter Haar, A.S. Protheroe, P.J. Friend, F. V. Gleeson, D.W. Cranston, R.R. Phillips, M.R. Middleton, The safety and feasibility of extracorporeal high-intensity focused ultrasound (HIFU) for the treatment of liver and kidney tumours in a Western population, Br. J. Cancer. 93 (2005) 890–895, https://doi.org/10.1038/sj.bjc.6602803.

[10] P.A. Deymier, Acoustic Metamaterials and Phononic Crystals, Springer, Berlin Heidelberg, Berlin, Heidelberg (2013), https://doi.org/10.1007/978-3-642-31232-8.

[11] M. Molerón, M. Serra-Garcia, C. Daraio, Acoustic Fresnel lenses with extraordinary transmission, Appl. Phys. Lett. 105 (2014) 11–16, https://doi.org/10.1063/1.4896276.

[12] A. Sukhovich, L. Jing, J.H. Page, Negative refraction and focusing of ultrasound in two-dimensional phononic crystals, Phys. Rev. B - Condens. Matter Mater. Phys. 77 (2008), https://doi.org/10.1103/PhysRevB.77.014301.

[13] A. Sukhovich, B. Merheb, K. Muralidharan, J. Vasseur, Y. Pennec, P. Deymier, J. Page, Experimental and Theoretical Evidence for Subwavelength Imaging in Phononic Crystals, Phys. Rev. Lett. 102 (2009), 154301, https://doi.org/10.1103/PhysRevLett.102.154301.

[14] A. Climente, D. Torrent, J. Sánchez-Dehesa, Sound focusing by gradient index sonic lenses, Appl. Phys. Lett. 97 (10) (2010) 104103.

[15] S. Zhang, R.K. Arya, S. Pandey, Y. Vardaxoglou, W. Whittow, R. Mittra, 3D-printed planar graded index lenses, IET Microwaves, Antennas Propag. 10 (2016) 1411–1419, https://doi.org/10.1049/iet-map.2016.0013.

[16] V. Romero-García, A. Cebrecos, R. Picó, V.J. Sánchez-Morcillo, L.M. Garcia-Raffi, J. V. Sánchez-Pérez, Wave focusing using symmetry matching in axisymmetric acoustic gradient index lenses, Appl. Phys. Lett. 103 (2013) 1–5, https://doi.org/10.1063/1.4860535.

[17] M. Chitnaduku Thippeswamy, S.A.R. Kuchibhatla, P. Rajagopal, Concentric shell gradient index metamaterials for focusing ultrasound in bulk media, Ultrasonics 114 (2021), 106424, https://doi.org/10.1016/j.ultras.2021.106424.

[18] Y. Li, G. Yu, B. Liang, X. Zou, G. Li, S. Cheng, J. Cheng, Three-dimensional ultrathin planar lenses by acoustic metamaterials, Sci. Rep. 4 (2014), https://doi.org/10.1038/srep06830.

[19] Y. Xie, A. Konneker, B.-I. Popa, S.A. Cummer, Tapered labyrinthine acoustic metamaterials for broadband impedance matching, Appl. Phys. Lett. 103 (20) (2013) 201906.

[20] Z. Liang, J. Li, Extreme acoustic metamaterial by coiling up space, Phys. Rev. Lett. 108 (2012), https://doi.org/10.1103/PhysRevLett.108.114301.

[21] A.O. Krushynska, F. Bosia, N.M. Pugno, Labyrinthine acoustic metamaterials with space-coiling channels for low-frequency sound control, Acta Acust. United with Acust. 104 (2018) 200–210, https://doi.org/10.3813/AAA.919161.

[22] S. Pérez-López, J.M. Fuster, P. Candelas, C. Rubio, Fractal lenses based on Cantor binary sequences for ultrasound focusing applications, Ultrasonics 99 (2019), 105967, https://doi.org/10.1016/j.ultras.2019.105967.

[23] G.Y. Song, B. Huang, H.Y. Dong, Q. Cheng, T.J. Cui, Broadband Focusing Acoustic Lens Based on Fractal Metamaterials, Sci. Rep. 6 (2016) 1–7, https://doi.org/10.1038/srep35929.

[24] Y. Xie, W. Wang, H. Chen, A. Konneker, B.I. Popa, S.A. Cummer, Wavefront modulation and subwavelength diffractive acoustics with an acoustic metasurface, Nat. Commun. 5 (2014) 1–5, https://doi.org/10.1038/ncomms6553.

[25] R. Fuentes-Domínguez, M. Yao, A. Colombi, P. Dryburgh, D. Pieris, A. Jackson-Crisp, D. Colquitt, A. Clare, R.J. Smith, M. Clark, Design of a resonant Luneburg lens for surface acoustic waves, Ultrasonics 111 (2021), 106306, https://doi.org/10.1016/j.ultras.2020.106306.

[26] D. Tarrazó-Serrano, C. Rubio, O.V. Minin, A. Uris, I.V. Minin, Ultrasonic focusing with mesoscale polymer cuboid, Ultrasonics 106 (2020), 106143, https://doi.org/10.1016/j.ultras.2020.106143.

[27] Y. Ruan, X. Liang, Z. Wang, T. Wang, Y. Deng, F. Qu, J. Zhang, 3-D underwater acoustic wave focusing by periodic structure, Appl. Phys. Lett. 114 (2019) 81908.

[28] H. Sun, S. Wang, S. Huang, L. Peng, Q. Wang, W. Zhao, Design and characterization of an acoustic composite lens with high-intensity and directionally controllable focusing, Sci. Rep. 10 (2020) 1–9, https://doi.org/10.1038/s41598-020-58092-6.

[29] E.B. Lima, V.H.S. Santos, A.L. Baggio, J.H. Lopes, J.P. Leão-Neto, G.T. Silva, An image formation model for ultrasound superresolution using a polymer ball lens, Appl. Acoust. 170 (2020), 107494.

[30] J.M. Fuster, P. Candelas, S. Castiñeira-Ibáñez, S. Pérez-López, C. Rubio, Analysis of fresnel zone plates focusing dependence on operating frequency, Sensors (Switzerland) 17 (2017) 1–10, https://doi.org/10.3390/s17122809.

[31] S. Pérez-López, J.M. Fuster, P. Candelas, C. Rubio, On the focusing enhancement of Soret zone plates with ultrasound directional transducers, Appl. Phys. Lett. 114 (2019), 224101.

[32] D. Tarrazó-Serrano, S. Castiñeira-Ibáñez, E. Sánchez-Aparisi, A. Uris, C. Rubio, MRI compatible planar material acoustic lenses, Appl. Sci. 8 (2018) 2634.

[33] L. Nie, D.A. Hutchins, L. Astolfi, T.P. Cooper, A.T. Clare, C. Adams, R.L. Watson, P. J. Thomas, D.M.J. Cowell, J.R. McLaughlan, S. Laureti, M. Ricci, S. Freear, A Metallic Additively-Manufactured Metamaterial for Enhanced Monitoring of Acoustic Cavitation-Based Therapeutic Ultrasound, Adv. Eng. Mater. 24 (4) (2022) 2100972.

[34] D. Tarrazó-Serrano, S. Pérez-López, P. Candelas, A. Uris, C. Rubio, Acoustic Focusing Enhancement In Fresnel Zone Plate Lenses, Sci. Rep. 9 (2019) 1–10, https://doi.org/10.1038/s41598-019-43495-x.

[35] D. Tarrazó-Serrano, C. Rubio, O.V. Minin, P. Candelas, I.V. Minin, Manipulation of focal patterns in acoustic Soret type zone plate lens by using reference radius/

phase effect, Ultrasonics 91 (2019) 237–241, https://doi.org/10.1016/j.ultras.2018.07.022.
[36] D.C. Calvo, A.L. Thangawng, M. Nicholas, C.N. Layman, Thin Fresnel zone plate lenses for focusing underwater sound, Appl. Phys. Lett. 107 (1) (2015) 014103.
[37] J. Zhu, J. Christensen, J. Jung, L. Martin-Moreno, X. Yin, L. Fok, X. Zhang, F. J. Garcia-Vidal, A holey-structured metamaterial for acoustic deep-subwavelength imaging, Nat. Phys. 7 (2011) 52–55, https://doi.org/10.1038/nphys1804.
[38] P. Laugier, G. Haïat, Introduction to the physics of ultrasound, Bone Quant, Ultrasound. (2011) 29–45.
[39] S. Laureti, D.A. Hutchins, L. Astolfi, R.L. Watson, P.J. Thomas, P. Burrascano, L. Nie, S. Freear, M. Askari, A.T. Clare, Trapped air metamaterials for ultrasonic sub-wavelength imaging in water, Sci. Rep. (2020) 1–29, https://doi.org/10.1038/s41598-020-67454-z.
[40] H.O. Agu, A. Hameed, G.J. Appleby-Thomas, D.C. Wood, The dynamic response of dense 3 dimensionally printed polylactic acid, J. Dyn. Behav. Mater. 5 (4) (2019) 377–386.
[41] M. Askari, D.A. Hutchins, P.J. Thomas, L. Astolfi, R.L. Watson, M. Abdi, M. Ricci, S. Laureti, L. Nie, S. Freear, R. Wildman, C. Tuck, M. Clarke, E. Woods, A.T. Clare, Additive manufacturing of metamaterials: A review, Addit. Manuf. 36 (2020), 101562, https://doi.org/10.1016/j.addma.2020.101562.
[42] L. Rabiner, R. Schafer, C. Rader, The Chirp z-Transform Algorithm, IEEE Trans. Audio Electroacoust. 17 (2) (1969) 86–92.
[43] X. Zhang, Z. Liu, Superlenses to overcome the diffraction limit, Nat. Mater. 7 (2008) 435–441, https://doi.org/10.1038/nmat2141.